Accuracy Check of GTD MER with Weighted Fringe Wave Using Fresnel Zone Number for Grazing Incidence and Slope Wave Diffraction

Maifuz Ali, Makoto Ando, Teruhiro Kinoshita, and Takashi Kuroki

Abstract – The reduction of the surface integration to line integration provides numerical computation time and resource savings. Modified edge representation (MER) is a unique concept for a complete definition of equivalent edge currents (EECs) for arbitrary points on the edge, including ones that do not satisfy the diffraction law. By using classical Keller-type diffraction coefficients in EECs, MER recovers the fringe wave (FW) contribution and has the enhanced accuracy of the order of the geometrical theory of diffraction (GTD). The line integration of MER EEC results in uniform and accurate fields everywhere, including geometrical boundaries at the caustics as inherent advantages and geometrical boundaries, such as the reflection shadow boundary (RSB) and incident shadow boundary (ISB). The authors have developed the applicability of MER and arrived at the advanced form of MER (new MER) in which FW components in EEC are weighted by the Fresnel zone number (FZN). This article demonstrates the higher accuracy and wider applicability of this method over GTD and the uniform geometrical theory of diffraction (UTD) for the canonical problem of a large circular disk where the rigorous solution is available. In grazing incidence as an extreme case, the FZN weighting effectively enhances the accuracy of GTD MER. It is also demonstrated that the inherent advantage of GTD MER over GTD and UTD in slope wave diffraction remain unchanged in new MER with this weighting.

1. Introduction

Physical optics (PO) is an asymptotic high-frequency numerical method on the basis of currents. In PO, the scattering fields are obtained by surface integration of surface electric current density. Because the reduction of the surface integral to line one provides numerical computation time savings, it has been investigated at length by many in both exact [1, 2] and asymptotic manners [3].

Stoke's theorem was used to obtain the reduction of the surface integral without the help of the image theory in [4]. A surface integral without an inner stationary phase point is directly reduced to line integration by modified edge representation (MER). The MER extended the concepts of [5] to general scattering problems, where the original edge is replaced by a fictitious edge, which is defined to satisfy the law of diffraction for a given direction of incidence and observation. The equivalent edge currents (EECs) for arbitrary incidence are completely determined at every point on the periphery by assuming the fictitious edge segment. This MER EEC technique consisting of classical Keller-type GTD diffraction coefficients [6, eq. (2)] is named *GTD MER* and takes account of the fringe wave (FW) component for accuracy with the level of GTD. The field singularities at the incident shadow boundary (ISB) and reflection shadow boundary (RSB) of GTD are suppressed after the MER line integration, and the superiority of GTD MER to GTD is demonstrated in [7, 8].

GTD MER contrasts with the uniform geometrical theory of diffraction (UTD) [9, 10] in two ways: the classical Keller-type diffraction coefficients with singularities are used that dispense with the Fresnel function; and corner diffraction is implemented without any extra techniques as demonstrated in [11] for dipole wave diffraction from rectangular and triangular plates. The important and inherent advantage of GTD MER for slope wave diffraction was also observed there. On the other hand, the degradation of accuracy of GTD MER at and near the shadow boundaries (SBs) for the grazing incidence was also reported as the unique and sole difficulty of GTD MER in [11–13], where the correction was also proposed as *new MER*; the FW is suppressed with the weighting by using the Fresnel zone number (FZN). The accuracy checks of new MER in detail, however, have not been conducted, mainly due to the lack of a rigorous solution for an electrically large object.

In this article, we investigate the accuracy of new MER for the scattering of a dipole wave from a large circular disk, where a rigorous solution is available [14]. The superiority of new MER to conventional high-frequency methods, such as PO, GTD, and UTD, is fully demonstrated. The accuracy and advantages of this method over UTD in evaluating slope wave are demonstrated with the method of moments (MoM)

Manuscript received 21 December 2019.

Maifuz Ali is with the International Institute of Informational Technology, Naya Raipur, Chhattisgarh 493661, India; e-mail: maifuzali@iiitnr.edu.in.

Makoto Ando is with the National Institute of Technology, 701-2, Higashi Asakawa, Hachioji, Tokyo 193-0834, Japan; e-mail: ando@kosen-k.go.jp.

Teruhiro Kinoshita is with the Tokyo Polytechnic University, 1583 Iiyama, Atsugi, Kanagawa 243-0297, Japan; e-mail: kinosita@t-kougei.ac.jp.

Takashi Kuroki is with Tokyo Metropolitan College of Industrial Technology, 1-10-40, Higashioi, Shinagawa, Tokyo 140-0011, Japan; e-mail: kuroki@metro-cit.ac.jp.

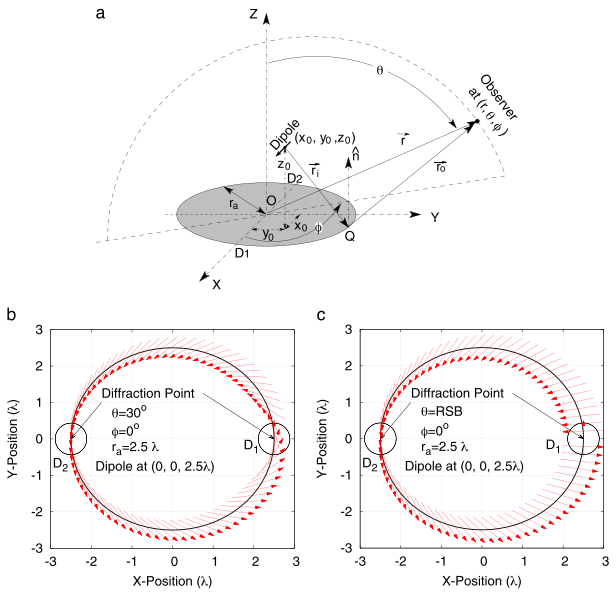

Figure 1. A circular disk illuminated by a dipole. (a) Coordinate system, (b) modified edges $\hat{\tau}$ along the periphery $\hat{e}$ of the disk for the observation at $\emptyset = 0^{\circ}$ and $\theta = 30^{\circ}$, and (c) for $\theta =$ RSB ($\approx 45^{\circ}$).

code (Wipl-D Pro V14 [15]), as the reference is also validated by the rigorous one [14].

2. MER EECs for the Computation of a Diffracted Field from a Circular Disk

The derivation of EECs is the key for surface to line integral reduction. A concept of MER, which extends the definition of EEC for diffraction points to those for general edge points, is detailed in [7, 8] for PO and FW components, respectively. Classical Keller's diffraction coefficients in [6] were used in GTD MER [11, 12].

Numerical verification and validation of GTD MER were conducted with Wipl-D [11–13, 16], and the advantages of GTD MER over UTD in terms of corner diffraction were discussed. A dipole along the x-axis is considered at (0, 0, 2.5λ) on a circular disk plate of the radius $r_a = 2.5\lambda$. The fictitious edge vector $\hat{\tau}$ along the real edge $\hat{e}$ for observation at $\emptyset = 0^{\circ}$ and $\theta = 30^{\circ}$ is shown in Figure 1b, and the observation at $\emptyset = 0^{\circ}$ and Θ = RSB is shown in Figure 1c. The fictitious edge $\hat{\tau}$ changes smoothly along the periphery of the scatterer to satisfy the diffraction law and coincides with the original edge e only at the points of edge diffraction $D_1(x = r_a, y = 0, z = 0)$ and $D_2(x = -r_a, y = 0, z = 0)$, as shown in Figure 1b. If the observer is close to the RSB (or ISB) and integration point passes through the diffraction point, $\hat{\tau}$ changes its sign abruptly and nearly perpendicular to $\hat{e}$ but at the diffraction point (D_1), and $\hat{\tau}$ coincides with $\hat{e}$, as shown in Figure 1c.

Field patterns due to a circular disk of radius $r_a = 2.5\lambda$ and infinitesimal dipole at (0, 0, 2.5λ) at the plane $\phi = 90^{\circ}$ are shown in Figure 2. In this figure, the results using a numerical electromagnetic code on the

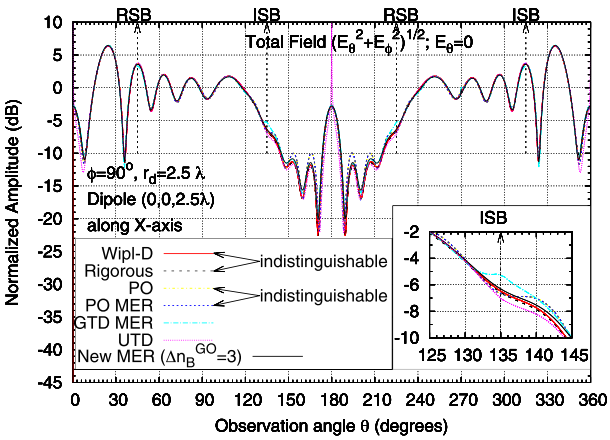

Figure 2. Total field (E_θ) patterns from a circular disk.

basis of the MoM (Wipl-D [15]) are also compared with those of rigorous analysis [14]. Two patterns (Wipl-D and rigorous) perfectly coincide with each other and are indistinguishable. The Wipl-D–simulated result will also be used as the indirect reference for a wider class of incidence, such as the slope one.

A. PO and PO MER

In PO, the scattering fields are obtained by surface integration of the surface current density $\left(2\hat{n} \times \overrightarrow{H^i}\right)$. In PO MER, on the other hand, diffracted fields are obtained by line integration of EECs along the periphery $(\hat{e})$ of the scatterer, while EECs are obtained from the PO diffraction coefficient D^{PO} in [11, table I], with respect to the fictitious edges $(\hat{\tau})$.

PO by surface integration and PO MER by line ingratiation are plotted in Figure 2, and these two patterns are also identical and indistinguishable. Although there are poles in the PO diffraction coefficient $\left(D^{\mathrm{PO}}\right)$ at the SBs (ISB and RSB), the fields by PO MER after integration are uniform and finite at the SBs. Also, the fields at and near the geometric caustics ($\phi = 0^{\circ}/360^{\circ}$ and 180°) are predicted perfectly. An interesting advantage of PO is observed at ISB, where PO approaches the rigorous one and is superior to other methods, such as GTD MER and UTD.

B. UTD, FW, and GTD MER

Fields computed by the UTD [9] are included in Figure 2. Although the field by UTD deviates at and near the caustics, the overall agreement with Wipl-D is excellent. The fields by UTD are superior to those by PO MER (or PO), except the field at and near the caustics. As UTD accounts for the FW, the difference between the results of UTD and PO MER comes from the FW effects.

The GTD diffraction coefficient D^{GTD} can be written in terms of PO $\left(D^{\mathrm{PO}}\right)$ and FW $\left(D^{\mathrm{FW}}\right)$ as follows [11]:

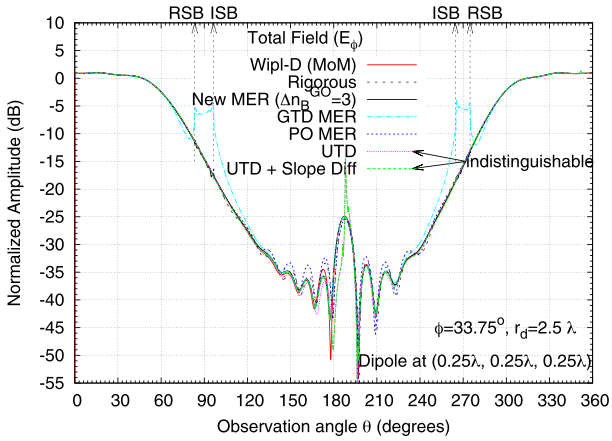

Figure 3. Total field (E_θ) patterns from a circular disk for grazing incidence.

$$\begin{bmatrix} D_s^{\mathrm{GTD}} & D_{sh}^{\mathrm{GTD}} \\ D_{xs}^{\mathrm{GTD}} & D_h^{\mathrm{GTD}} \end{bmatrix} = \begin{bmatrix} D_s^{\mathrm{PO}} & D_{sh}^{\mathrm{PO}} \\ D_{xs}^{\mathrm{PO}} & D_h^{\mathrm{PO}} \end{bmatrix} + \mathrm{EYE}^{\mathrm{FW}}\left(\frac{\Delta n^{\mathrm{GO}}}{\Delta n_B^{\mathrm{GO}}}\right) \begin{bmatrix} D_s^{\mathrm{FW}} & D_{sh}^{\mathrm{FW}} \\ D_{xs}^{\mathrm{FW}} & D_h^{\mathrm{FW}} \end{bmatrix} \tag{1}$$

$\mathrm{EYE}^{\mathrm{FW}}$, introduced in (2), is unity for GTD MER. Actually, the FW in [11, table I] has been used widely, simply because of its finiteness in contrast with the infinities of GTD and asymptotic PO of the Keller type. In GTD MER, diffraction coefficients in (1) are calculated not for the real edge ($\hat{e}$) but for the modified edge ($\hat{\tau}$) introduced in [11]. The field patterns by GTD MER are shown in Figure 2, and overall, it is superior to other methods, such as PO MER and UTD.

3. Errors of the GTD MER Field Near the SBs for Grazing Incidence

If the source is very close to the scatterer, the separation between RSB and ISB becomes smaller. The dipole is located at (0.25λ, 0.25λ, and 0.25λ) along the x-axis and the $\emptyset$ component of field ($E_\emptyset$) at the $\emptyset = 33.75^\circ$ plane are shown in Figure 3. This pattern is compared with the rigorous analysis. It is observed that at the angles far from SBs, GTD MER matches with the rigorous analysis very well when compared with PO MER. For the observer near SBs on the other hand, GTD MER deviates from reference results, while PO MER matches almost perfectly.

This unique error in GTD MER at and near the SB for the grazing incidence comes from the FW integration in MER. In the specific situation of the observer and the source, the modified edge ($\hat{\tau}$) along the periphery ($\hat{e}$) changes its sign abruptly when it crosses the point of diffraction, as shown in Figure 1c. The EECs in PO MER are insensitive to the sign $\hat{e}$, while those in FW MER are sign sensitive [7, 8], and the abrupt change of sign brings about errors in FW MER. The FW EECs near the point of abrupt change were

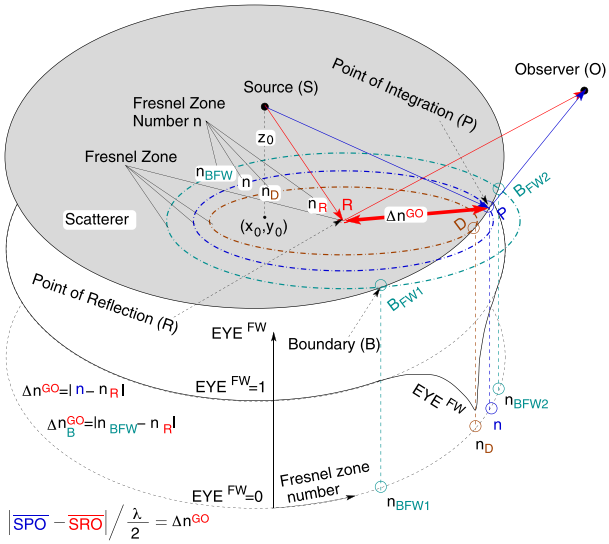

Figure 4. Fresnel zone and weighting function to modify FW.

modified, especially for the observer near SBs for the grazing incidence [11].

4. Modification of FW MER

A. FZN for Suppressing the FW

A modification of FW on the basis of FZN (n) is proposed in [11, 12]. For new MER, a weighting function in (1) is redefined to suppress FW components given by

$$\begin{aligned} &\mathrm{EYE}^{\mathrm{FW}}\left(\frac{\Delta n^{\mathrm{GO}}}{\Delta n_B^{\mathrm{GO}}}\right) \\ &\quad = \frac{1}{2}\left\{1 - \cos\left(\frac{\Delta n^{\mathrm{GO}}}{\Delta n_B^{\mathrm{GO}}}\pi\right)\right\} \text{ for } \Delta n^{\mathrm{GO}} < \Delta n_B^{\mathrm{GO}}(=3) \\ &\quad = 1 \text{ for } \Delta n^{\mathrm{GO}} < \Delta n_B^{\mathrm{GO}}(=3) \end{aligned} \tag{2}$$

where $\Delta n^{\mathrm{GO}}(=|n - n_R|)$ is the difference in FZN between the point of geometrical optics (GO) reflection and the point of integration, as is indicated in Figure 4. As usual, in the case of general wireless communication systems, for a given positions of the source (S) and the observer (O), we can define the FZN for the arbitrary point P in space as $n = 2|L|/\lambda$, where L is the path length difference between the direct path SO and the diverted path SPO. Let us imagine the intersection of Fresnel zones and the scatterer; any point on the disk is associated with the FZN, as is depicted in Figure 4. Actually, the modified edge $\hat{\tau}$ is parallel to the contour of the equal FZN [17].

B. $\mathrm{EYE}^{\mathrm{FW}}$ and New FW MER Field

When the observer is close to ISB (or RSB) and the integration point approaches the diffraction point,

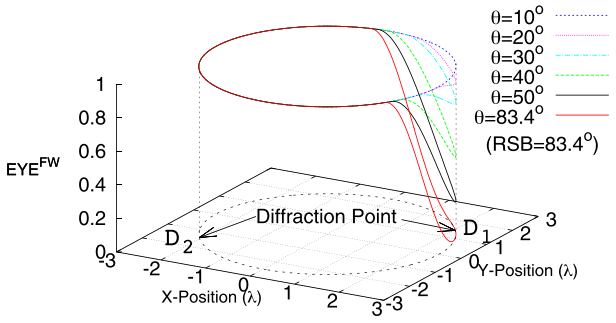

Figure 5. Weighting values $(\mathrm{EYE}^{\mathrm{FW}})$ along the periphery of a circular disk.

$\Delta n^{\mathrm{GO}} \to 0$, and the weighting approaches zero. On the contrary, if the observer is far away from ISB (or RSB) or the point of integration is far away from the diffraction points $\Delta n^{\mathrm{GO}} \geq \Delta n_B^{\mathrm{GO}}$, the weighting approaches unity.

The weighting values $\mathrm{EYE}^{\mathrm{FW}}$ for $\Delta n_B^{\mathrm{GO}} = 3$, and the observation at $\phi = 33.75^{\circ}$ and $\theta = 10^{\circ}$, 20°, 30°, 40°, and 50° and $\theta = 83.4^{\circ} (\approx \mathrm{RSB})$ are shown in Figure 5. Fields by new MER with FW weighted by $\mathrm{EYE}^{\mathrm{FW}}$ are shown in Figure 3, and they agree very well with the rigorous one in all angles of observations.

5. Slope Diffraction

Next, the dipole is turned 45° with the x-axis and 135° with the z-axis, and the total field pattern (E_θ) at $\emptyset = 0^{\circ}$ plane is shown in Figure 6. The incident field at the diffraction point $D_1(r_1, 0, 0)$ is zero, but the slope of the incident field is nonzero $\left(\frac{\partial E_\theta^i}{\partial n} \neq 0\right)$. Wipl-D–simulated results, validated by the rigorous solution in Figure 2, will be used as the reference for the slope diffraction. The results by new MER are almost identical with GTD MER, and both match well with the Wipl-D results in all angles of observations. The field computed by UTD of [9] is included in Figure 6, which has disagreement with the Wipl-D. Adding the slope-diffracted field [10] with UTD, we obtain the results shown as UTD + slope diff. This recovers the slope effects and shows good agreement with Wipl-D. Thus, the slope effects should be treated separately in UTD, but UTD + slope diff still has disadvantages at geometrical caustics.

As in the planar case, PO MER is numerically indistinguishable with PO surface integration. PO MER, GTD MER, and hence new MER include the effects of the slope of the incident field, which is verified in Figure 6.

6. Conclusion

This article provides a comparative study among PO surface integration, PO MER, UTD, GTD MER, and new MER. GTD MER recovers many disadvantages of PO, GTD, and UTD. The errors or degradation of GTD MER around SBs, especially for grazing incidence are suppressed in new MER with FZN weighting. The rigorous solution developed for the large circular disk provides the reference in the accuracy check. It is also demonstrated that for slope wave effect, new MER and GTD MER do not need any extra computation, such as UTD.

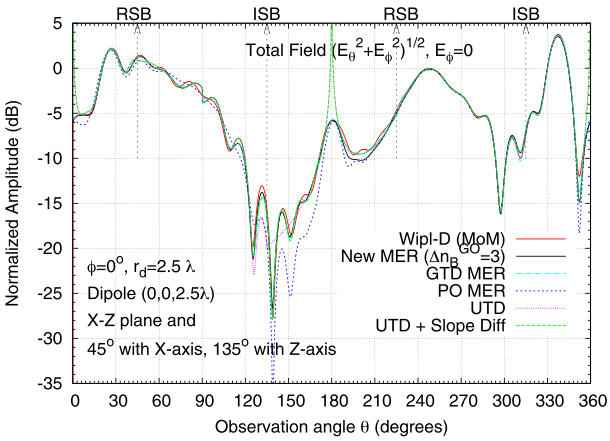

Figure 6. Total field (E_θ) patterns from a circular disk.

7. References

1. J. S. Asvestas, "Line Integrals and Physical Optics. Part I and II. The Conversion of the Kirchhoff Surface Integral to a Line Integral," *Journal of the Optical Society of America A*, **2**, 6, June 1985, pp. 891–902.
2. P. M. Johansen and O. Breinbjerg, "An Exact Line Integral Representation of the Physical Optics Scattered Field: The Case of a Perfectly Conducting Polyhedral Structure Illuminated by Electric Hertzian Dipoles," *IEEE Transactions on Antennas and Propagation*, **43**, 7, July 1995, pp. 689–696.
3. A. Michaeli, "Elimination of Infinities in Equivalent Edge Currents, Pt. 2: Physical Optics Components," *IEEE Transactions on Antennas and Propagation*, **34**, 8, August 1986, pp. 1034–1037.
4. M. Ando, T. Murasaki, and T. Kinoshita, "Elimination of False Singularities in GTD Equivalent Edge Currents," *IEEE Proceedings H - Microwaves, Antennas and Propagation*, **138**, 4, August 1991, pp. 289–296.
5. Fathi A. Sikta, Walter D. Burnside, Tai-Tseng Chu, and Leon Peters, Jr., "First-Order Equivalent Current and Corner Diffraction Scattering From Flat Plate Structures," *IEEE Transactions on Antennas and Propagation*, **31**, 4, July 1983, pp. 584–589.
6. J. B. Keller, "Geometrical Theory of Diffraction," *Journal of the Optical Society of America*, **52**, 2, February 1962, pp. 116–130.
7. T. Murasaki and M. Ando, "Equivalent Edge Currents by the Modified Edge Representation: Physical Optics Components," *IEICE Transactions on Electronics*, **E75-c**, 5, May 1992, pp. 617–624.
8. T. Murasaki, M. Sato, Y. Inasawa, and M. Ando, "Equivalent Edge Currents for Modified Edge Representation of Flat Plates: Fringe Wave Components," *IEICE Transactions on Electronics*, **E76-c**, 9, September 1993, pp. 1412–1419.
9. R. G. Kouyoumjian and P. H. Pathak, "A Uniform Geometrical Theory of Diffraction for an Edge in a Perfectly Conducting Surface," *Proceedings of the IEEE*, **62**, 11, November 1974, pp. 1448–1461.

10. Constantine A. Balanis, *Advanced Engineering Electromagnetics*, New York, Wiley, 1989.
11. M. Ali, T. Kohama, and M. Ando, "Modified Edge Representation (MER) Consisting of Keller's Diffraction Coefficients with Weighted Fringe Waves and Its Localization for Evaluation of Corner Diffraction," *IEEE Transactions on Antennas and Propagation*, **63**, 7, July 2015, pp. 3158–3167.
12. M. Ali and M. Ando, "New Expressions of Fringe Wave in EEC Consisting of Keller's Diffraction Coefficient," Proceedings of 36th General Assembly and Scientific Symposium of the International Union of Radio Science, Beijing, China, August 2014, page number B06.2.
13. M. Ando and M. Ali, "Full Use of Keller's GTD Coefficients in Method of Equivalent Edge Currents for Corner-, Slope- and Grazing Incidence-Diffraction" in International Symposium on Electromagnetic Theory, San Diego, CA, May 2019, page number E04b-4.
14. T. Kuroki, T. Shibazaki, and T. Kinoshita, "Current Distribution on a Conductive Circular Disk Induced by Dipole Source Located at Arbitrary Position," *IEICE Transactions on Electronics*, **E96-c**, 1, January 2013, pp. 3–10.
15. B. M. Kolundzija, J. S. Ognjanovic, and T. K. Sarkar, *WIPL-D: Electromagnetic Modeling of Composite Metallic and Dielectric Structures: Software and User's Manual*, Boston, Artech House, 2000.
16. M. Ali and M. Ando, **"**Computation of Slope Diffraction by Modified Edge Representation (MER) Equivalent Edge Currents (EECs) Line Integration" in URSI Asia-Pacific Radio Science Conference, New Delhi, India; March 2019, page number Tu-BO6-4.
17. K. Sakina and M. Ando, "Mathematical Derivation of Modified Edge Representation for Reduction of Surface Radiation Integral," *IEICE Transactions on Electronics*, **E84-c**, 1, January 2001, pp. 74–83.